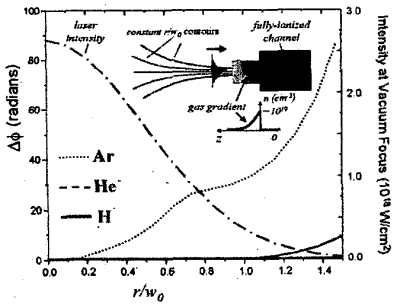

JTuB3 Fig. 3. Calculation of the radial phase (referenced to r = 0) suffered by a pulse traversing the cell entrance region, due to ionization effects. The pulse must propagate through this region of neutral gas before entering the fully-ionized channel (inset). The graph shows that for a *0.15 J, 50 fs, 0.8 μm* laser pulse, the accumulated radial phase is negligible for channels in Hydrogen and Helium, but becomes large for Ar channels with density $n(z = 0) = 3 \times 10^{19}\ cm^{-3}$. A large variation in radial phase represents significant curvature to the phase front, and is thus indicative of severe ionization-induced defocusing.

tensity ($\sim 0.6 \times 10^{18}$ W/cm^2) required for efficient LWF generation. However, the pulse will then ionize the back-fill gas before reaching the channel, even in Helium. We have therefore built a differentially-pumped cell, which still enables the channel to be generated in a region of uniform density, but reduces the extent of neutral gas in the entrance/exit regions to *<1 mm*, as demonstrated by the measurements in Fig. 2. Our simulations of intense pulse propagation through this inhomogeneous ionizing gas profile, using ADK ionization, relativistic cold fluid and Maxwell equations,[4] (Fig 3) predict focused intensity 10^{18} W/cm^2 can be coupled with minimal distortion.

1. C.G. Durfee, III and H.M. Milchberg, "Light pipe for high intensity laser pulses," Phys. Rev. Lett. 71, 2409 (1993).
2. E.W. Gaul, S.P. LeBlanc, H. Langhoff, N.H. Matlis, M.C. Downer, "Plasma channels in doubly ionized helium", in *Conference on Lasers and Electro-Optics,* OSA Technical Digest (Optical Society of America, Washington DC, 1999), p. 213.
3. E.W. Gaul, S.P. LeBlanc, A.R. Rundquist, R. Zgazaj, H. Langhoff, and M.C. Downer, "Production and characterization of a fully ionized He plasma channel", Appl. Phys. Lett. 77, 4112 (2000).
4. N. Andreev, M.V. Chegotov, M.C. Downer, E.W. Gaul, N.H. Matlis, A.A. Pogosova, and A.R. Rundquist, "Propagation of intense laser pulses through inhomogeneous ionizing gas profiles," IEEE Transactions on Plasma Science 28, 1090 (2000).

JTuB4 **Invited** **11:15 am**

Relativistic Nonlinear Optics: From the Atomic to the Quark Structure of Matter

Gerard Mourou, Univ. of Michigan, USA

Today laser optics is standing on the threshold of new physics frontiers. Until recently, traditional optics and nonlinear optics have addressed phenomena in the eV regime, focusing essentially on the study of the atomic structure of matter. It is today possible to produce intensities in the range of 10^{18}–10^{22} W/cm^2, that is 10^4–10^6 higher than was possible only few years ago. These intensities could even reach in the future values as high as 10^{29} W/cm^2. These gargantuan intensities could make possible the exploration of much deeper strata of the structure of matter. Photon-photon colliders or $\gamma\gamma$ colliders. which are planned on all linear colliders, are excellent examples. They will be implemented to look at the properties of the Higgs boson(s), supersymmetric particle production and physics beyond the Standard Model.

At 10^{18}W/cm^2 and above, laser-matter interaction is dominated by the relativistic and ultra-relativistic character of the electron oscillating in the laser field and leads to fundamentally new physical effects. Among the effects are relativistic harmonic generation, relativistic self focusing and "and the generation of very large field gradients. These effects extend the field of laser physics from the eV to the GeV with the generation of x-ray, γ-rays, neutrons, positrons, MeV protons, 100 MeV electrons. Tomorrow even much higher electron energy in the TeV to PeV could be reached leading to a new high energy physics paradigm.

After a discussion of the laser intensity upper limit, we will give an overview of the field of relativistic optics that could be considered as the second wind of nonlinear optics. In particular we will give examples of applications to, fusion energy, astrophysics, nuclear physics, high energy physics and gravitational physics.

JTuB5 **11:45 am**

MeV Proton Generation with a kHz Femtosecond Laser

A. Thoss, G. Korn, N. Zhavoronkov, T. Elsaesser, Max-Born-Institut für Nichtlineare Optik und Kurzzeitspektroskopie, Max-Born-Str. 2A, D-12489 Berlin, Germany, Email: thoss@mbi-berlin.de

M. Richardson, also at School of Optics & CREOL, Univ. Central Florida, Orlando (FL), USA

M. Faubel, Max-Planck-Institut für Strömungsforschung, Göttingen, Germany

Recent experimental investigations of laser-plasmas produced by high-intensity (>10^{18}W/cm^2) ultra-short pulse lasers from solid targets have shown the generation of copious fluxes of collimated MeV protons, predominantly from the rear-side of the target[1–4]. The intensity scaling of both the proton energy and their conversion efficiency from laser light appears to be more than linear, prompting suggestions that at higher laser intensities, such collimated beams of multi-MeV protons might be used for proton tomography, proton therapy for cancer treatment and other similar applications. So far these protons have only been generated with multi-stage CPA (chirped pulse amplification) laser systems operating in either the single shot regime, or at a few Hz. However, the peak intensity capabilities of high repetition-rate ultra-short (<100 fs) Ti:Sapphire laser systems are now reaching levels where they too may be used to investigate this proton generation. We report here, the first experiments made in this regime.

To accomplish this, we needed to employ a target geometry that would allow accurate replenishment of the target material, presenting a virgin target surface to each laser pulse with a spatial precision of a few microns. In previous studies, the proton emission originates from thin layers of water vapor or hydrocarbons deposited on the backside of the target, (resulting from vacuum chamber contaminants). In the experiments described here, we use as a target, a microscopic stream of water, some 10–50 μm in diameter,[5] a target already rich in hydrogen atoms, and flowing sufficiently fast that it is unlikely to accumulate contaminants from the vacuum chamber. Moreover whereas nearly all previous investigations have used massive planar targets, in the present case we use a thin cylindrical target having a diameter similar in size to the laser focal size. This microscopic target geometry has possible implications for the interpretation of the generation mechanisms of the protons themselves and the subsequent directionality of their emission.

The laser used in the present experiments consists of a mode-locked Ti:Sapphire a regenerative amplifier followed by a double pass booster amplifier providing compressed 50 fs pulses at a wavelength of 780 nm ($\Delta\lambda \sim 25$ nm) with a maximum average power of ~2 W. The peak intensity on target is currently in excess of 3×10^{16} W/cm^2. The addition of a deformable mirror in the near future will significantly increase this value. The jet target being used is of the Faubel design.[6] This produces a stable continuous jet of water >4.6 mm long from the nozzle (for a 30 μm dia. jet) and >1.7 mm long for a 10 μm jet. The laser beam is focused onto the jet with a 70 mm focal length lens, producing a laser spot size, currently, of 10 μm (FWHM).

Angular distribution and spectral energy measurements of the proton emission is being made with the use of CR-39 track detectors. Two detectors are located ~3 cm from the target, one monitoring the proton emission emanating from the rear of the target, subtending a total solid angle of ~80 degrees in the forward direction of the laser beam (Fig. 1). The second detector monitors protons accelerated from the front surface of the target on one side of the focusing lens, detecting particles coming from the target at angles of 10° to 90° from the backward direction of the laser beam. The angular distribution of the protons has been studied under a range of operating parameters. At lower intensities (mid 10^{15} W/cm^2), the forward-going emission has an angular width of 20°–30°, and contains $\sim 2.6 \times 10^6$ protons.

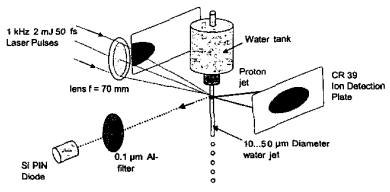

JTuB5 Fig. 1. Experimental set-up for the detection of protons.

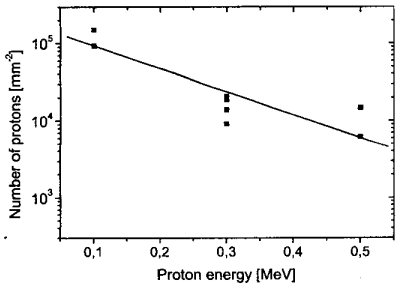

JTuB5 Fig. 2. Proton energy spectrum at an intensity of 3×10^{16} W/cm^2. Exponential regression gives $kT_{hot} \approx 300$ keV.

Spectrometric measurements are also being made of the energy distribution of the protons using various thicknesses of thin Al and mylar foils as energy filters. Fig. 2 shows a proton energy spectrum deduced from these measurements for a laser intensity of 3×10^{16} W/cm^2, indicating its origin from an electron burst having a temperature in the range of 300 keV. These measurements are in line with the expectations of scaling laws derived from earlier experiments.[7,8]

Continuing improvements to the high repetition-rate femtosecond laser system will provide much higher intensities, in excess of 10^{18} W/cm^2. In this regime, proton generation will be much more efficient, and their maximum energy will be in the multiple—MeV range. Whether these particle fluxes will be sufficient to stimulate interest in their use for proton tomography or proton cancer therapy may not be sure. However they will, without doubt be enough to initiate studies of the impact of short bursts of protons on solid-state and biological matter. The availability of synchronised femtosecond optical pulses, either at the laser wavelength, or at other wavelengths in IR, visible or UV range, derived from this wavelength by nonlinear optical methods, will provide many ways for time-resolved pump-probe determinations of reversible and non reversible structural changes.

References

1. A. Maksimchuk, S. Gu, K. Flippo, D. Umstadter, Phys. Rev. Lett. **84**, 4108 (2000).
2. A. Clark et. al., Phys. Rev. Lett. **84**, 670 (2000).
3. R.A. Snavely et al., Phys. Rev. Lett. **85**, 2945 (2000).
4. A.J. Mackinnon et al., Phys. Rev. Lett. **86**, 1769 (2001).
5. A. Thoss, M. Richardson, G. Korn, M. Faubel, & T. Elsaesser, (to be published).
6. M. Faubel, in "Photoionization and Photodetachment", Ed. C.Y. Ng, World Scientific, Singapore, p. 634–690 (2000).
7. A. Clark et al., Phys. Rev. Lett. **85**, 1654 (2000).
8. S. Wilks et al, Phys. Plasmas **8**, 542 (2001).

JTuC 10:15 am–12:00 pm
Room: 203

Photonic Crystal Lasers and Defects

Leslie Kolodziejski, MIT, USA, Presider

JTuC1 Invited **10:15 am**

Photonic Band Gap Materials: A Semiconductor for Light

Professor Sajeev John, Department of Physics, 60 Saint George Street, University of Toronto, Toronto, Ontario CANADA M5S 1A7, Email: john@physics.utoronto.ca

I review and discuss the role of three-dimensional light localization in the development of integrated optics on a photonic crystal micro-chip. The control and selective inhibition of spontaneous emission in a three dimensional photonic band gap material offers the possibility of developing novel active devices on such a chip.

JTuC2 **10:45 am**

Two-Dimensional Photonic Crystal Ring Laser

Se-Heon Kim, Han-Youl Ryu, Hong-Gyu Park, Guk-Hyun Kim, and Yong-Hee Lee, Department of physics, Korea Advanced Institute of Science and Technology, Taejon 305-701, Korea, Email: kalt@kaist.ac.kr

Jeong-Soo Kim, Telecommunication Basic Research laboratory, Electronics and Telecommunications Research Institute, Taejon, 305-600, Korea

Recently, groups world wide have investigated photonic crystal structures for future photonic integrated circuit applications.[1] The existence of photonic band gaps in photonic crystals results in various applications such as lasers, light emitting diodes, planar waveguides, and channel drop filters. In this report, we propose and demonstrate lasing action in ring-type resonators defined by two-dimensional photonic crystals on a free-standing slab with InGaAsP active layers emitting at 1.55 μm.

Free-standing photonic crystal slab structures are fabricated by using electron-beam lithography, chemically-assisted ion-beam etching, and undercut wet etching. The SEM image of a fabricated structure are shown in Fig. 1(a). Lattice constant of this laser sample is $a \sim 570$ nm and the air hole radius is $\sim 0.36\ a$. In fact, the photonic crystal ring lasers with various ring sizes are fabricated. The fabricated structures are pulse-pumped by a 980-nm laser diode at room temperature. The pulse width is 10 ns and duty cycle is 1%. The pump spot size is about 8 μm, which is sufficiently large to cover the entire ring pattern. Lasing actions from samples with various ring sizes are observed.

A spectrum of the aforementioned ring laser above threshold shows the lasing wavelength of 1620 nm. An L-L curve (the collected power at the lasing wavelength versus incident peak pump power) in Fig. 2 shows a threshold pump power

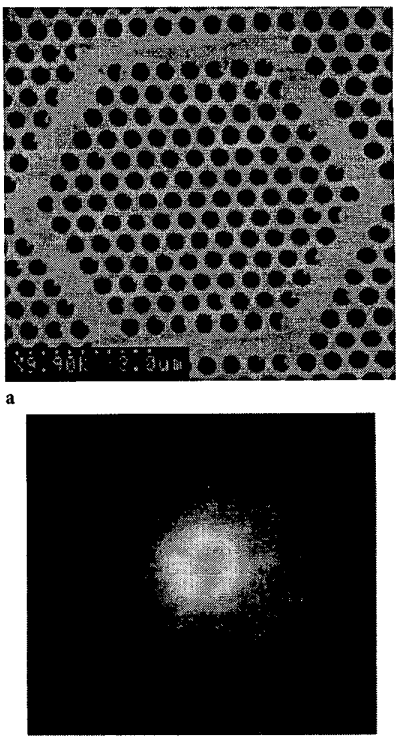

JTuC2 Fig. 1. (a) SEM image of photonic crystal ring laser ($a \sim 570$ nm, $r/a = 0.36$). (b) CCD near-field image.

of ~3 mW. As the incident pump power decreases to below threshold, another peak close to the lasing mode shows up (insets of Fig. 2). This existence of nonlasing mode is the general characteristic in the microdisk lasers.[2] So, the lasing mode of our ring resonator originate from the true ring-type mode. The CCD near-field image in Fig. 1(b) also shows that the laser is mainly emitted from the ring regions. The Q factor of the ring resonator is measured from the below threshold linewidth, which sets the lower bound as ~2000.

The photonic crystal ring laser consists of 6

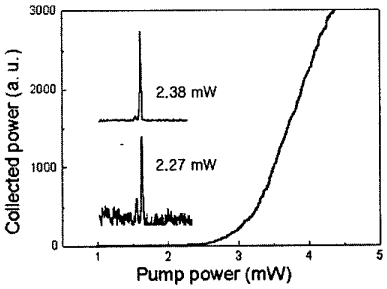

JTuC2 Fig. 2. L-L curve (the collected power at the lasing wavelength versus incident peak pump power). Insets are the spectra with the incident pump power below threshold at 2.38 mW and 2.27 mW respectively.